Characterization of random features of chaotic eigenfunctions in unperturbed basis

Jiaozi Wang* and Wen-ge Wang†
Department of Modern Physics, University of Science and Technology of China, Hefei 230026, China

(Received 29 January 2018; revised manuscript received 11 June 2018; published 25 June 2018)

In this paper we study random features manifested in components of energy eigenfunctions of quantum chaotic systems, given in the basis of unperturbed, integrable systems. Based on semiclassical analysis, particularly on Berry's conjecture, it is shown that the components in classically allowed regions can be regarded as Gaussian random numbers in a certain sense, when appropriately rescaled with respect to the average shape of the eigenfunctions. This suggests that when a perturbed system changes from integrable to chaotic, deviation of the distribution of rescaled components in classically allowed regions from the Gaussian distribution may be employed as a measure for the "distance" to quantum chaos. Numerical simulations performed in the Lipkin-Meshkov-Glick model and the Dicke model show that this deviation coincides with the deviation of the nearest-level-spacing distribution from the prediction of random-matrix theory. Similar numerical results are also obtained in two models without classical counterpart.

DOI: 10.1103/PhysRevE.97.062219

I. INTRODUCTION

A commonly held view in the field of quantum chaos is that energy eigenfunctions (EFs) of chaotic systems should show certain random feature [1–4], though their Hamiltonian matrices are deterministic and some of them even may show a sparse structure. This property has vast applications in various fields [5–15]. In particular, it is of relevance to thermalization [16–24], a topic which has attracted renewed interest in recent years.

According to Berry's conjecture, for EFs of chaotic systems expressed in the configuration space, their components in classically allowed regions can be regarded as being given from certain Gaussian random numbers [1]. Based on this conjecture, it is natural to expect that, when expanded in the bases of unperturbed integrable systems, the EFs should show certain random features as well within appropriate regions. Indeed, numerical simulations reveal such a feature for the main bodies of EFs (see, e.g., Ref. [25]). However, a more detailed study showed that the distribution of components of EFs usually exhibits notable deviation from the Gaussian distribution, which is predicted the random-matrix theory (RMT) (see, e.g., Ref. [5]).

More recently, numerical simulations show that, if EFs are rescaled with respect to their average shape, the above-discussed deviation can be considerably reduced [26,27]. This gives a clue to a solution to a long-standing problem in the field of quantum chaos, that is, in which way statistical properties of EFs may be employed to give a quantitative measure for the "distance" to chaos. The above-mentioned numerical simulations suggest that deviation of the distribution of rescaled components of EFs from the Gaussian distribution should be a candidate for such a measure of "distance." However, at present, the situation is not completely clear, because in some cases this measure shows notable deviations from results obtained from statistical properties of spectra, e.g., from deviation of the nearest-level-spacing distribution from the prediction of the RMT [26,27].

In this paper, based on semiclassical analysis, particularly on the Berry's conjecture, we study random features manifested in components of EFs of chaotic systems in integrable bases. Our analysis shows that the distribution of the components in classically allowed regions indeed should have a Gaussian form, under a rescaling procedure which is more appropriate than that adopted in Refs. [26,27]. Our numerical simulations performed for the Lipkin-Meshkov-Glick (LMG) model and the Dicke model show that, adopting this new rescaling procedure, deviation of the distribution of components from the Gaussian distribution coincides quite well with that obtained from the statistics of spectra. We also study some models without any classical counterpart and find similar results.

The paper is organized as follows. In Sec. II a detailed semiclassical analysis is carried out for random features manifested in components of EFs of chaotic systems in integrable bases. Numerical simulations in two models with classical counterparts are discussed in Sec. III. Then in Sec. IV we discuss numerical simulations performed in two models without classical counterpart. Finally, conclusions and a discussion are given in Sec. V.

II. RANDOM FEATURES OF CHAOTIC EFS

In Sec. II A based on semiclassical analysis we discuss random features of chaotic EFs. Then, making use of results obtained, we discuss a quantitative characterization of the random feature in Sec. II B.

*wangjz@ustc.edu.cn
†wgwang@ustc.edu.cn

A. Semiclassical analysis of chaotic EFs

Consider a quantum system, which has an f-dimensional classical counterpart, with a Hamiltonian

$$H = H_0 + \lambda V, \tag{1}$$

where H_0 indicates the Hamiltonian of an integrable system and V is a perturbation. Within a certain regime of the parameter λ, the classical counterpart of the system H undergoes a chaotic motion. In this section, we consider a chaotic system H. In terms of action-angle variables, H_0 is written as

$$H_0 = \boldsymbol{d}\cdot\boldsymbol{I} + c_0, \tag{2}$$

where $\boldsymbol{I} = (I_1, I_2, \ldots, I_f)$ is the action variable, $\boldsymbol{d}$ is a parameter vector, $\boldsymbol{d} = (d_1, d_2, \ldots, d_f)$, and c_0 is a constant parameter.

In the quantum case, we use $|\boldsymbol{n}\rangle$ to denote the eigenbasis of $\boldsymbol{I}$, with $\boldsymbol{I}|\boldsymbol{n}\rangle = \boldsymbol{I}_{\boldsymbol{n}}|\boldsymbol{n}\rangle$, where $\boldsymbol{n} = (n_1, n_2, \ldots, n_f)$ is an integer vector and $\boldsymbol{I}_{\boldsymbol{n}} = \boldsymbol{n}\hbar$. The Hamiltonian H_0 has a diagonal form in this basis with eigenvalues denoted by $E^0_{\boldsymbol{n}}$,

$$H_0|\boldsymbol{n}\rangle = E^0_{\boldsymbol{n}}|\boldsymbol{n}\rangle. \tag{3}$$

We use $|E_\alpha\rangle$ to denote eigenstates of H with eigenvalues E_α in energy order,

$$H|E_\alpha\rangle = E_\alpha|E_\alpha\rangle. \tag{4}$$

The expansion of $|E_\alpha\rangle$ in the basis $|\boldsymbol{n}\rangle$ is written as

$$|E_\alpha\rangle = \sum_{\boldsymbol{n}} C_{\alpha\boldsymbol{n}}|\boldsymbol{n}\rangle, \tag{5}$$

with $C_{\alpha\boldsymbol{n}} = \langle\boldsymbol{n}|E_\alpha\rangle$. Below we discuss random features manifested in the components $C_{\alpha\boldsymbol{n}}$ and their statistical properties in chaotic systems.

In terms of the wave functions of $|E_\alpha\rangle$ and $|\boldsymbol{n}\rangle$ in the momentum space, denoted by $\psi_\alpha(\boldsymbol{p})$ and $\psi^0_{\boldsymbol{n}}(\boldsymbol{p})$, respectively, the components $C_{\alpha\boldsymbol{n}}$ are written as

$$C_{\alpha\boldsymbol{n}} = \int \left[\psi^0_{\boldsymbol{n}}(\boldsymbol{p})\right]^* \psi_\alpha(\boldsymbol{p})\, d\boldsymbol{p}. \tag{6}$$

Generically, a wave function $\psi_\alpha(\boldsymbol{p})$ can be written in the following form:

$$\psi_\alpha(\boldsymbol{p}) = A_\alpha(\boldsymbol{p})\sqrt{\Pi_\alpha(\boldsymbol{p})}, \tag{7}$$

where $\Pi_\alpha(\boldsymbol{p})$ indicates local average of $|\psi_\alpha(\boldsymbol{p})|^2$. Then $C_{\alpha\boldsymbol{n}}$ is written as

$$C_{\alpha\boldsymbol{n}} = \int A_\alpha(\boldsymbol{p})\left[\psi^0_{\boldsymbol{n}}(\boldsymbol{p})\right]^* \sqrt{\Pi_\alpha(\boldsymbol{p})}\, d\boldsymbol{p}. \tag{8}$$

According to the Berry's conjecture [1], in a chaotic system the quantity $A_\alpha(\boldsymbol{p})$ should have random phases. This implies that the components $C_{\alpha\boldsymbol{n}}$ can be effectively regarded as some random numbers.

In realistic physical models, the average shape of $|C_{\alpha\boldsymbol{n}}|^2$ is usually not uniform with respect to the perturbed and unperturbed energies. Due to this nonuniformity, the statistical distribution of the components $C_{\alpha\boldsymbol{n}}$ cannot have a Gaussian shape [5]. But, if they are rescaled such that the effect of average shape of EFs is appropriately taken into account, it should be possible for their distribution to have a Gaussian form. Below we derive a semiclassical expression for the average shape of $|C_{\alpha\boldsymbol{n}}|^2$ that is suitable for this purpose.

The Wigner function supplies a useful tool in semiclassical analysis of eigenstates. We use $\psi_\alpha(\boldsymbol{r})$ and $\psi^0_{\boldsymbol{n}}(\boldsymbol{r})$ to indicate the wave functions of $|E_\alpha\rangle$ and $|\boldsymbol{n}\rangle$ in the coordinate space, respectively. The Wigner function corresponding to $\psi_\alpha(\boldsymbol{r})$, denoted by $W_\alpha(\boldsymbol{p},\boldsymbol{q})$, is written as

$$W_\alpha(\boldsymbol{p},\boldsymbol{q}) = \frac{1}{(2\pi\hbar)^f}\int_{-\infty}^{\infty} \psi^*_\alpha\left(\boldsymbol{q}+\frac{\boldsymbol{r}}{2}\right)\psi_\alpha\left(\boldsymbol{q}-\frac{\boldsymbol{r}}{2}\right)e^{i\,\boldsymbol{p}\cdot\boldsymbol{r}/\hbar}\, d\boldsymbol{r}, \tag{9}$$

and similarly for the Wigner function corresponding to $\psi^0_{\boldsymbol{n}}(\boldsymbol{r})$, denoted by $W^0_{\boldsymbol{n}}(\boldsymbol{p},\boldsymbol{q})$. As is known, in a chaotic system the averaged Wigner function, with the average taken within certain small regions of the phase space, has the following expression [1,2,28,29]:

$$\overline{W}_\alpha(\boldsymbol{p},\boldsymbol{q}) = \frac{\delta[H(\boldsymbol{p},\boldsymbol{q}) - E_\alpha]}{S(E_\alpha)}, \tag{10}$$

where $S(E)$ represents the area of an energy surface with $H(\boldsymbol{p},\boldsymbol{q}) = E$,

$$S(E) = \int d\boldsymbol{p}\, d\boldsymbol{q}\, \delta[E - H(\boldsymbol{p},\boldsymbol{q})]. \tag{11}$$

Equation (10) gives that

$$\Pi_\alpha(\boldsymbol{p}) = \frac{1}{S(E_\alpha)}\int \delta[E_\alpha - H(\boldsymbol{p},\boldsymbol{q})]\, d\boldsymbol{q}. \tag{12}$$

Equation (10) implies that most eigenstates within a narrow energy window in a chaotic system should have shapes close to each other. Therefore, when computing the average shape of $|C_{\alpha\boldsymbol{n}}|^2$ for the purpose discussed above, one may perform an average within such a narrow energy window. For the convenience in discussion, we write a coarse-grained δ function as $\delta_\epsilon(E)$,

$$\delta_\epsilon(E) = \begin{cases} \frac{1}{\epsilon} & E \in [-\frac{\epsilon}{2}, \frac{\epsilon}{2}], \\ 0 & \text{otherwise}, \end{cases} \tag{13}$$

where ϵ is a small parameter. The choice of energy window ϵ should satisfy the following requirements: It is small in the classical case such that the energy surface almost does not change within the window, while it is sufficiently large in the quantum case such that many energy levels are included within the window.

Then the average shape of EFs, denoted by $\langle|C_{\alpha\boldsymbol{n}}|^2\rangle$, is computed by

$$\langle|C_{\alpha\boldsymbol{n}}|^2\rangle = \frac{1}{N_{E_\alpha}}\sum_{\alpha'}|C_{\alpha'\boldsymbol{n}}|^2\delta_\epsilon(E_{\alpha'} - E_\alpha), \tag{14}$$

where

$$N_{E_\alpha} = \sum_{\alpha'}\delta_\epsilon(E_{\alpha'} - E_\alpha). \tag{15}$$

In order to derive an explicit expression for $\langle|C_{\alpha\boldsymbol{n}}|^2\rangle$, we make use of the following well-known expression of $|C_{\alpha\boldsymbol{n}}|^2$:

$$|C_{\alpha\boldsymbol{n}}|^2 = (2\pi\hbar)^f \int d\boldsymbol{p}\, d\boldsymbol{q}\, W_\alpha(\boldsymbol{p},\boldsymbol{q})W^0_{\boldsymbol{n}}(\boldsymbol{p},\boldsymbol{q}). \tag{16}$$

Let us divide the phase space into small cells, denoted by c_σ with a label σ, each having a volume $\delta\Omega$, and meanwhile keep

the ratio $\delta\Omega/\hbar^f$ large such that there are many quantum states "lying" within each small cell. Then $|C_{\alpha \boldsymbol{n}}|^2$ is written as

$$|C_{\alpha \boldsymbol{n}}|^2 = (2\pi\hbar)^f \sum_\sigma \int_{c_\sigma} d\boldsymbol{p}\, d\boldsymbol{q}\, W_\alpha(\boldsymbol{p},\boldsymbol{q}) W_{\boldsymbol{n}}^0(\boldsymbol{p},\boldsymbol{q}). \quad (17)$$

Substituting Eq. (17) into Eq. (14) and performing the summation over the perturbed states $|E_{\alpha'}\rangle$, one gets that

$$\langle |C_{\alpha \boldsymbol{n}}|^2 \rangle = (2\pi\hbar)^f \sum_\sigma \int_{c_\sigma} d\boldsymbol{p}\, d\boldsymbol{q} \langle W_\alpha(\boldsymbol{p},\boldsymbol{q})\rangle W_{\boldsymbol{n}}^0(\boldsymbol{p},\boldsymbol{q}), \quad (18)$$

where $\langle W_\alpha(\boldsymbol{p},\boldsymbol{q})\rangle$ indicates the average of $W_\alpha(\boldsymbol{p},\boldsymbol{q})$ over perturbed states within a small energy window ϵ. As many energy levels are included within the window ϵ, $\langle W_\alpha(\boldsymbol{p},\boldsymbol{q})\rangle$ should vary slowly within each small cell c_σ, such that

$$\langle W_\alpha(\boldsymbol{p},\boldsymbol{q})\rangle \simeq \langle W_\alpha(\boldsymbol{p}_\sigma,\boldsymbol{q}_\sigma)\rangle \quad \text{for } (\boldsymbol{p},\boldsymbol{q}) \in c_\sigma, \quad (19)$$

where $(\boldsymbol{q}_\sigma,\boldsymbol{p}_\sigma)$ indicates the center of c_σ. Then Eq. (18) gives that

$$\langle |C_{\alpha \boldsymbol{n}}|^2 \rangle \simeq (2\pi\hbar)^f \sum_\sigma \langle W_\alpha(\boldsymbol{p}_\sigma,\boldsymbol{q}_\sigma)\rangle \overline{W}_{\boldsymbol{n}}^0(\boldsymbol{p}_\sigma,\boldsymbol{q}_\sigma)\delta\Omega, \quad (20)$$

where $\overline{W}_{\boldsymbol{n}}^0(\boldsymbol{p}_\sigma,\boldsymbol{q}_\sigma)$ represents the average of the Wigner function of the integrable system within the cell c_σ,

$$\overline{W}_{\boldsymbol{n}}^0(\boldsymbol{p}_\sigma,\boldsymbol{q}_\sigma) = \frac{1}{\delta\Omega}\int_{c_\sigma} W_{\boldsymbol{n}}^0(\boldsymbol{p},\boldsymbol{q})\, d\boldsymbol{p}\, d\boldsymbol{q}. \quad (21)$$

Due to the classical smallness and quantum mechanical largeness of the energy windows ϵ discussed previously, $\langle W_\alpha(\boldsymbol{p},\boldsymbol{q})\rangle$ in Eq. (18) obeys Eq. (10) in an approximate way, with

$$\langle W_\alpha(\boldsymbol{p},\boldsymbol{q})\rangle \simeq \overline{W}_\alpha(\boldsymbol{p},\boldsymbol{q}), \quad (22)$$

and its dependence on ϵ can be neglected. It is known that [1]

$$\overline{W}_{\boldsymbol{n}}^0(\boldsymbol{p},\boldsymbol{q}) = \frac{\delta[\boldsymbol{I}(\boldsymbol{p},\boldsymbol{q}) - \boldsymbol{I}_{\boldsymbol{n}}]}{(2\pi)^f}. \quad (23)$$

Substituting Eqs. (22) and (23) into Eq. (20) and noting that the smallness of the cells c_σ enables one to change the summation over σ back to the integration over phase space, and one gets the following semiclassical expression:

$$\langle |C_{\alpha \boldsymbol{n}}|^2 \rangle \simeq \hbar^f\ \Pi(E_\alpha, \boldsymbol{I}_{\boldsymbol{n}}), \quad (24)$$

where

$$\Pi(E,\boldsymbol{I}) = \frac{S(E,\boldsymbol{I})}{S(E)}, \quad (25)$$

$$S(E,\boldsymbol{I}) = \int d\boldsymbol{p}\, d\boldsymbol{q}\, \delta[E - H(\boldsymbol{p},\boldsymbol{q})]\delta[\boldsymbol{I} - \boldsymbol{I}(\boldsymbol{p},\boldsymbol{q})]. \quad (26)$$

Here $S(E,\boldsymbol{I})$ indicates the overlap of the energy surface of $H(\boldsymbol{p},\boldsymbol{q}) = E$ and the torus of $\boldsymbol{I}(\boldsymbol{p},\boldsymbol{q}) = \boldsymbol{I}$. Since Eq. (10) works for classically allowed regions only, so does Eq. (24). Sometimes, quantities like $\Pi(E,\boldsymbol{I})$ are called classical analog of averaged EFs [26,30,31].

Finally, we consider rescaled components denoted by $R_{\alpha \boldsymbol{n}}$, defined by

$$R_{\alpha \boldsymbol{n}} = \frac{C_{\alpha \boldsymbol{n}}}{\sqrt{\langle |C_{\alpha \boldsymbol{n}}|^2\rangle}}. \quad (27)$$

Discussions given above show that the quantities $R_{\alpha \boldsymbol{n}}$ have a random feature with a Gaussian distribution with mean zero. Note that $\langle |R_{\alpha \boldsymbol{n}}|^2\rangle = 1$ according to Eq. (27).

B. A measure for "distance" to quantum chaos

Let us use $f(R)$ to denote the distribution of $R_{\alpha \boldsymbol{n}}$. According to results given above, for a chaotic system, $f(R)$ should have a Gaussian form,

$$f(R) = f_G(R), \quad (28)$$

where $f_G(R)$ is the Gaussian distribution,

$$f_G(R) = \frac{1}{\sqrt{2\pi}} \exp(-R^2/2). \quad (29)$$

In the RMT, the Gaussian distribution is predicted directly for components of EFs [4]. But, for Hamiltonians in realistic models with chaotic classical counterparts, as discussed above, it is the distribution of the rescaled components $R_{\alpha \boldsymbol{n}}$ that should have a Gaussian form. On the other hand, in a nearly integrable system, the quantity $A_\alpha(\boldsymbol{p})$ on the right-hand side of Eq. (8) does not have random phases and EFs with close energies may have quite different shapes. As a result, the distribution $f(R)$ in nearly integrable systems should usually show notable deviation from $f_G(R)$.

The above discussions suggest that deviation of $f(R)$ from $f_G(R)$ may be employed as an measure for the "distance" to quantum chaos. In order to quantitatively characterize the deviation, one may consider a quantity Δ_{EF} defined by

$$\Delta_{EF} = \int |I_f(R) - I_{f_G}(R)|\, dR, \quad (30)$$

where $I_f(R)$ and $I_{f_G}(R)$ indicate the cumulative distributions of $f(R)$ and $f_G(R)$, respectively, e.g., $I_f(R) = \int_{-\infty}^R dr f(r)$. As is well known, cumulative distributions usually exhibit fewer fluctuations compared with the origin distributions.

In the field of quantum chaos, the most-often used criterion for quantum chaos is given by statistical properties of spectra, e.g., by closeness of the nearest-level-spacing distribution $P(s)$ to the prediction of RMT [4]. It is known that the distribution $P_W(s)$, which is obtained from Wigner's surmise,

$$P_W(s) = \frac{\pi}{2} s \exp\left(-\frac{\pi}{4}s^2\right), \quad (31)$$

gives a good approximation to the nearest-level-spacing distribution of the Gaussian orthogonal ensemble in the large size limit. Quantitatively, the above-discussed closeness can be characterized by the quantity Δ_E,

$$\Delta_E = \int |I_P(s) - I_{P_W}(s)|\, ds, \quad (32)$$

where $I_P(s)$ and $I_{P_W}(s)$ are cumulative distributions of $P(s)$ and $P_W(s)$, respectively.

In previous numerical simulations, deviation of the distribution of another rescaled components, denoted by $R'_{\alpha \boldsymbol{n}}$, from the Gaussian distribution was studied as a measure for the "distance" to chaos, where $R'_{\alpha \boldsymbol{n}} = C_{\alpha \boldsymbol{n}}/\sqrt{\langle |C_{\alpha \boldsymbol{n}}|^2\rangle'}$ [26,27,32]. Here, in the computation of $\langle |C_{\alpha \boldsymbol{n}}|^2\rangle'$, in addition to an average over perturbed states with energies close to E_α, a further

average is taken over unperturbed states $|\boldsymbol{n}'\rangle$ with unperturbed energies close to $E^0_{\boldsymbol{n}}$ by a small quantity ϵ_0. Specifically,

$$\langle |C_{\alpha \boldsymbol{n}}|^2 \rangle' = \sum_{\alpha', \boldsymbol{n}'} \frac{|C_{\alpha' \boldsymbol{n}'}|^2}{N_{E_\alpha} N_{E_{\boldsymbol{n}}}} \delta_\epsilon (E_{\alpha'} - E_\alpha) \delta_{\epsilon_0} (E_{\boldsymbol{n}'} - E_{\boldsymbol{n}}), \quad (33)$$

where N_{E_α} is defined in Eq. (15) and

$$N_{E_{\boldsymbol{n}}} = \sum_{\boldsymbol{n}'} \delta_{\epsilon_0} (E_{\boldsymbol{n}'} - E_{\boldsymbol{n}}). \quad (34)$$

It was found that in some cases (not rare) in which the classical counterparts undergo chaotic motion and the distributions $P(s)$ are quite close to $P_W(s)$, the distributions of $R'_{\alpha \boldsymbol{n}}$, denoted by $g(R')$, deviate notably from the Gaussian distribution.

In view of the semiclassical analysis given in the previous section, it is understandable that deviation of $g(R')$ from $f_G(R')$ may be larger than that of $f(R)$ from $f_G(R)$. In fact, unperturbed basis states $|\boldsymbol{n}\rangle$ with close energies $E^0_{\boldsymbol{n}}$ may correspond to quite different values of $\boldsymbol{I}_{\boldsymbol{n}}$, while meanwhile, according to Eq. (24), the values of $\langle |C_{\alpha \boldsymbol{n}}|^2 \rangle$ of those $\boldsymbol{n}$, for which $\boldsymbol{I}_{\boldsymbol{n}}$ are far from each other, are usually quite different. As a result, taking the average over unperturbed basis states with close $E^0_{\boldsymbol{n}}$ may drive the distribution of rescaled components away from the Gaussian distribution.

Therefore, in order to obtain rescaled components that have a Gaussian distribution, no average should be taken over the unperturbed energies $E^0_{\boldsymbol{n}}$. We would remark that, when the torus of $\boldsymbol{I} = \boldsymbol{I}_{\boldsymbol{n}}$ does not change rapidly with $\boldsymbol{n}$, an average over a neighborhood of $\boldsymbol{n}$ is allowed. We did not mention this averaging procedure in the above discussion because it is unnecessary in the derivation of Eq. (24).

III. NUMERICAL SIMULATIONS IN TWO MODELS WITH CLASSICAL COUNTERPARTS

In order to test the above analytical results, numerical simulations have been performed in two models possessing classical counterparts: the LMG model and the Dicke model. In this section, we first briefly discuss the two models, and then present numerical results about the distribution $f(R)$ and about the suggested "distance" to chaos, namely, Δ_{EF}, in comparison with other "distances."

A. Models

The first model we employ is a three-orbital LMG model [33]. This model is composed of Ω particles, occupying three energy levels labeled by $r = 0,1,2$, each with Ω degeneracy. Here we are interested in the collective motion of this model, for which the dimension of the Hilbert space is $\frac{1}{2}(\Omega+1)(\Omega+2)$. We use ϵ_r to denote the energy of the rth level, and, for brevity, we set $\epsilon_0 = 0$. The Hamiltonian of the model, in the form in Eq. (1), has [7]

$$H_0 = \epsilon_1 K_{11} + \epsilon_2 K_{22}, \quad (35)$$

$$V = \sum_{t=1}^{4} \mu_t V^{(t)}, \quad (36)$$

where

$$V^{(1)} = K_{10}K_{10} + K_{01}K_{01}, \quad V^{(2)} = K_{20}K_{20} + K_{02}K_{02},$$
$$V^{(3)} = K_{21}K_{20} + K_{02}K_{12}, \quad V^{(4)} = K_{12}K_{10} + K_{01}K_{21}. \quad (37)$$

Here the operators K_{rs} are defined by

$$K_{rs} = \sum_{\gamma=1}^{\Omega} a^\dagger_{r\gamma} a_{s\gamma}, \quad r,s = 0,1,2, \quad (38)$$

where $a^\dagger_{r\gamma}$ and $a_{r\gamma}$ are fermionic creation and annihilation operators obeying the usual anticommutation relations.

For symmetric states, the operators K_{rs} can be written in terms of bosonic creation and annihilation operators $b^\dagger_r$ and b_r [34],

$$K_{rs} = b^\dagger_r b_s, \quad K_{r0} = K^\dagger_{0r} = b^\dagger_r \sqrt{\Omega - b^\dagger_1 b_1 - b^\dagger_2 b_2} \quad (39)$$

for $r,s = 1,2$. Under the transformation,

$$b^\dagger_r = \sqrt{\frac{\Omega}{2}}(q_r - i p_r), \quad b_r = \sqrt{\frac{\Omega}{2}}(q_r + i p_r) \quad (40)$$

for $r = 1,2$, it is easy to verify that q_r and p_s obey the following commutation relation:

$$[q_r, p_s] = \frac{i}{\Omega} \delta_{rs}. \quad (41)$$

Hence, $1/\Omega$ plays the role of an effective Planck constant:

$$\hbar_{\text{eff}} = \frac{1}{\Omega}. \quad (42)$$

It is straightforward to find that the classical counterpart of model has the following Hamiltonian [5,7]:

$$H(\boldsymbol{p},\boldsymbol{q}) = H_0(\boldsymbol{p},\boldsymbol{q}) + \lambda V(\boldsymbol{p},\boldsymbol{q}), \quad (43)$$

where

$$H_0(\boldsymbol{p},\boldsymbol{q}) = \frac{\epsilon'_1}{2}(p_1^2 + q_1^2) + \frac{\epsilon'_2}{2}(p_2^2 + q_2^2),$$
$$V(\boldsymbol{p},\boldsymbol{q}) = \mu'_1(q_1^2 - p_1^2)(1 - G/2) + \mu'_2(q_2^2 - p_2^2)(1 - G/2)$$
$$+ \frac{\mu'_3}{\sqrt{2}}\left[(q_2^2 - p_2^2)q_1 - 2q_2 p_1 p_2\right]\sqrt{1 - G/2}$$
$$+ \frac{\mu'_4}{\sqrt{2}}\left[(q_1^2 - p_1^2)q_2 - 2q_1 p_1 p_2\right]\sqrt{1 - G/2}, \quad (44)$$

with $G = q_1^2 + p_1^2 + q_2^2 + p_2^2 \leqslant 2$. Here $\epsilon'_1 = \epsilon_1\Omega, \epsilon'_2 = \epsilon_2\Omega$, $\mu'_1 = \mu_1\Omega^2, \mu'_2 = \mu_2\Omega^2, \mu'_3 = \mu_3\Omega^2$, and $\mu'_4 = \mu_4\Omega^2$. In our numerical simulations, we set $\epsilon'_1 = 44.1, \epsilon'_2 = 64.5$, $\mu'_1 = 62.1, \mu'_2 = 70.2, \mu'_3 = 76.5$, and $\mu'_4 = 65.7$. Under this choice of the parameters, for a fixed value of λ, different values of Ω correspond to a same classical counterpart.

The second model is a single-mode Dicke model [35,36], which describes the interaction between a single bosonic mode and a collection of N two-level atoms. The system can be described in terms of the collective operator $\mathbf{J}$ for the N atoms, with

$$J_z = \sum_{i=1}^{N} s_z^{(i)}, \quad J_\pm = \sum_{i=1}^{N} s_\pm^{(i)}, \quad (45)$$

where $s_{\pm}^{(i)} = s_x^{(i)} \pm i s_y^{(i)}$ and $s_{x(y,z)}^{(i)}$ are Pauli matrices divided by 2 for the ith atom. The Dicke Hamiltonian is written as [36]

$$H = \omega_0 J_z + \omega a^\dagger a + \frac{\lambda}{\sqrt{N}}\mu(a^\dagger + a)(J_+ + J_-), \tag{46}$$

which can also be written in the form of $H = H_0 + \lambda V$. The operator J_z and $J_\pm$ obey the usual commutation rules for the angular momentum,

$$[J_z, J_\pm] = \pm J_\pm, \quad [J_+, J_-] = 2J_z. \tag{47}$$

The Hilbert space of this model is spanned by vectors $|j,m\rangle$ with $m = -j, -j+1, \ldots, j-1, j$, known as Dicke states. They are eigenstates of $\boldsymbol{J}^2$ and J_z, with $J_z|j,m\rangle = m|j,m\rangle$ and $\boldsymbol{J}^2|j,m\rangle = j(j+1)|j,m\rangle$. Below we take j as its maximal value, $j = N/2$; it is a constant of motion, since $[\boldsymbol{J}^2, H] = 0$. Another conserved observable in the Dicke model is the parity Π, given by $\Pi = \exp(i\pi\hat{N})$, where $\hat{N} = a^\dagger a + J_z + j$ is an operator for the "excitation number," counting the total number of excitation quanta in the system. In our numerical study, we consider the subspace with $\Pi = +1$.

Making use of the Holstein-Primakoff representation of the angular momentum operators,

$$J_+ = b^\dagger\sqrt{2j - b^\dagger b}, \quad J_- = \sqrt{2j - b^\dagger b}\, b,$$
$$J_z = (b^\dagger b - j), \tag{48}$$

where b and $b^\dagger$ are bosonic operators satisfying $[b, b^\dagger] = 1$, the Hamiltonian can be further written in the following form:

$$H = \omega_0(b^\dagger b - j) + \omega a^\dagger a + \lambda\mu(a^\dagger + a)\left(b^\dagger\sqrt{1 - \frac{b^\dagger b}{2j}} + \sqrt{1 - \frac{b^\dagger b}{2j}}\, b\right). \tag{49}$$

We write Fock states related to $a^\dagger$ and $b^\dagger$ as $|n_a\rangle$ and $|n_b\rangle$, respectively, for which

$$a^\dagger a|n_a\rangle = n_a|n_a\rangle, \quad b^\dagger b|n_b\rangle = n_b|n_b\rangle. \tag{50}$$

According to Eq. (48), n_b should be truncated at $(n_b)_{\max} = N$. In numerical simulations, we set $(n_a)_{\max} = N$. Other parameters are $\omega_0 = \omega = 1/N$ and $\mu = 1/N$. Under the transformation

$$\begin{cases} b^\dagger = \sqrt{\frac{N}{2}}(q_1 - ip_1), & b = \sqrt{\frac{N}{2}}(q_1 + ip_1), \\ a^\dagger = \sqrt{\frac{N}{2}}(q_2 - ip_2), & a = \sqrt{\frac{N}{2}}(q_2 + ip_2), \end{cases} \tag{51}$$

one finds that

$$[q_r, p_s] = \frac{i}{N}\delta_{rs} \tag{52}$$

for $r = 1,2$ and, hence, gets an effective Planck constant

$$\hbar_{\text{eff}} = \frac{1}{N}. \tag{53}$$

The Hamiltonian of the classical counterpart of the model is written as

$$H(\boldsymbol{p},\boldsymbol{q}) = H_0(\boldsymbol{p},\boldsymbol{q}) + \lambda V(\boldsymbol{p},\boldsymbol{q}), \tag{54}$$

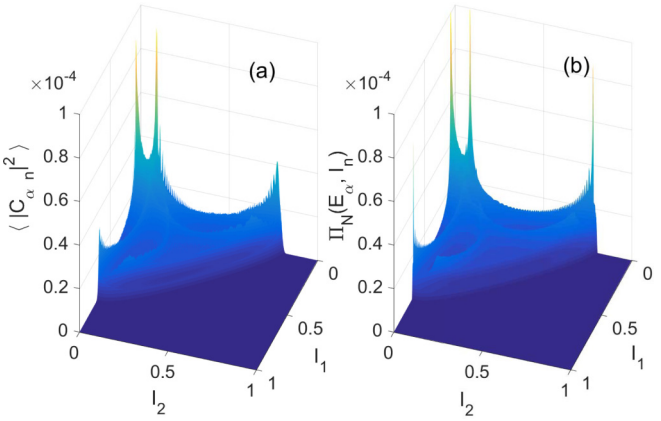

FIG. 1. (a) The average shape of EFs, $\langle|C_{\alpha n}|^2\rangle$, in the chaotic regime of the LMG model with $\Omega = 500$ and $\lambda = 1$. The average is taken over 500 EFs of $|E_\alpha\rangle$ with $\epsilon = 0.4175$. (b) $\Pi_N(E_\alpha, \boldsymbol{I_n})$, which is the normalized $\Pi(E_\alpha, \boldsymbol{I_n})$, as a classical analog of $\langle|C_{\alpha n}|^2\rangle$ [see Eq. (24)].

where

$$H_0(\boldsymbol{p},\boldsymbol{q}) = \frac{1}{2}\left(q_1^2 + p_1^2 + q_2^2 + p_2^2 - 1\right),$$
$$V(\boldsymbol{p},\boldsymbol{q}) = 2q_1q_2\sqrt{1 - \frac{q_1^2 + p_1^2}{2}}. \tag{55}$$

B. Numerical results

In this section, we discuss results of numerical simulations performed in the LMG model and the Dicke model. We first test validity of the semiclassical result given in Eq. (24). As seen in Figs. 1 and 2, the average shape $\langle|C_{\alpha n}|^2\rangle$ and its classical analog $\Pi(E_\alpha, \boldsymbol{I_n})$ indeed show similar features in these two models. We have computed the difference between the two shapes, given by

$$d_c = \sum_{\boldsymbol{n}} |\langle|C_{\alpha n}|^2\rangle - \Pi_N(E_\alpha, \boldsymbol{I_n})|, \tag{56}$$

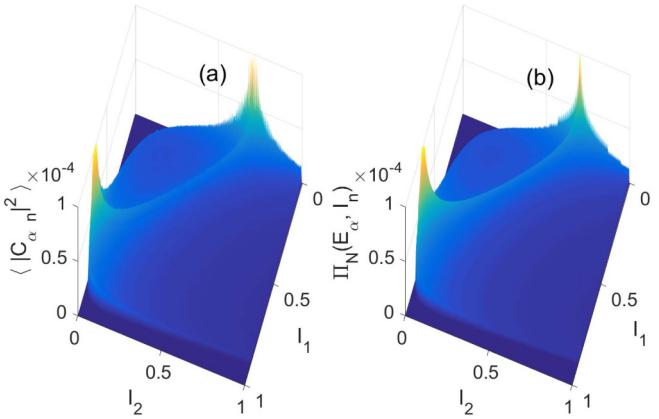

FIG. 2. Similar to Fig. 1, but for the Dicke model with $N = 500$, $\lambda = 1$, and $\epsilon = 0.007$.

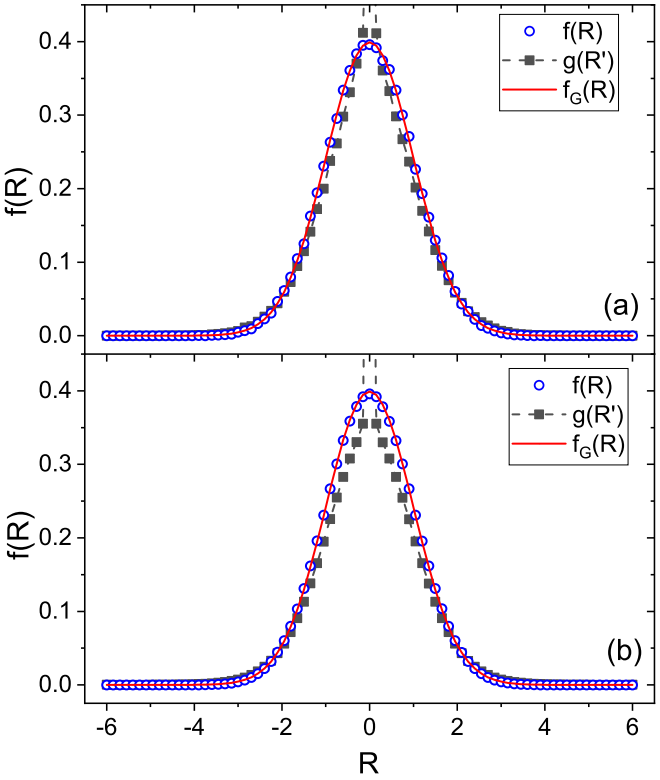

FIG. 3. The distribution $f(R)$ (open circles) and $g(R')$ (solid blocks with dashed lines) for $\lambda = 1$ in the LMG model with (a) $\Omega = 80$ and (b) $\Omega = 1000$. The solid curves indicate the Gaussian distribution $f_G(R)$.

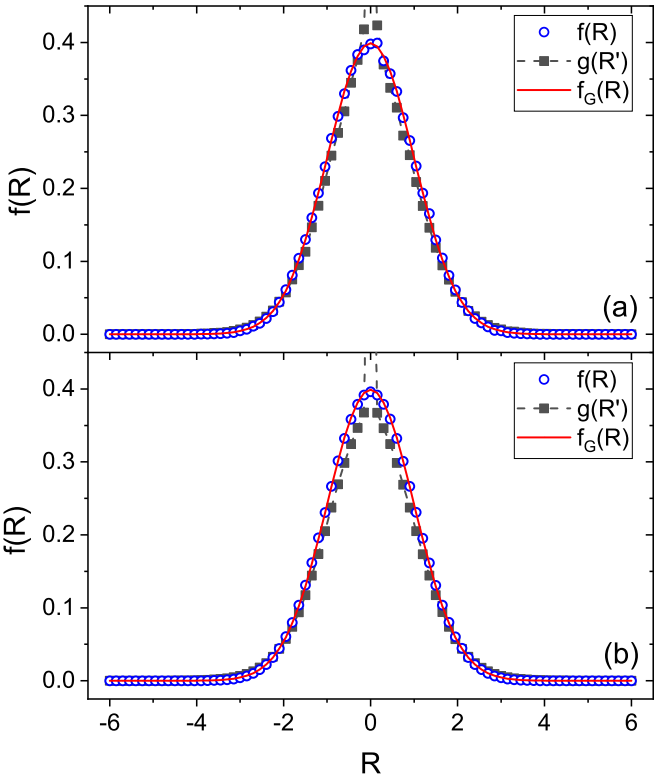

FIG. 4. Similar to Fig. 3, but for the Dicke model with $\lambda = 1$, (a) $N = 80$, (b) $N = 1000$.

where $\Pi_N(E_\alpha, \boldsymbol{I_n})$ is the normalized $\Pi(E_\alpha, \boldsymbol{I_n})$. We found that $d_c = 0.065$ in the LMG model and $d_c = 0.08$ in the Dicke model.

Then, we discuss properties of the distribution $f(R)$ for components $R_{\alpha \boldsymbol{n}}$ in classically allowed regions with $\Pi(E_\alpha, \boldsymbol{I_n}) \neq 0$. We found that this distribution is indeed quite close to the Gaussian form $f_G(R)$, when the underlying classical dynamics is chaotic, as illustrated in Figs. 3 and 4 with $\lambda = 1$. In the computation of $f(R)$, 100 EFs in the middle energy region were used. The energy windows ϵ are as follows: In the LMG mode, $\epsilon \approx 3$ for $\Omega = 80$ and $\epsilon \approx 0.02$ for $\Omega = 1000$, in contrast to the total energy domain $\Delta E = 64.5$ in the unperturbed system; in the Dicke mode, $\epsilon \approx 0.2$ for $N = 80$ and $\epsilon \approx 0.002$ for $N = 1000$, in contrast to the total energy domain $\Delta E = 2$.

For comparison, we have also computed the distribution $g(R')$ given by another rescaling procedure, in which an average over unperturbed states is also performed (see discussion in Sec. IIB). In this rescaling procedure, as discussed in Refs. [26,31], the average shape of EFs is expected to have the following semiclassical approximation:

$$\langle |C_{\alpha \boldsymbol{n}}|^2 \rangle' \simeq \frac{S(E, E_0)}{(2\pi\hbar)^f \rho(E) \rho_0(E_0)}, \tag{57}$$

where $\rho_0(E_0)$ and $\rho(E)$ are the density of states of the two systems H_0 and H, respectively, and $S(E, E_0)$ indicates the overlap of the perturbed energy surface of $H = E$ and the unperturbed energy surface of $H_0 = E_0$,

$$S(E, E_0) = \int d\boldsymbol{q}\, d\boldsymbol{p}\, \delta[E - H(\boldsymbol{p}, \boldsymbol{q})] \delta[E_0 - H_0(\boldsymbol{p}, \boldsymbol{q})]. \tag{58}$$

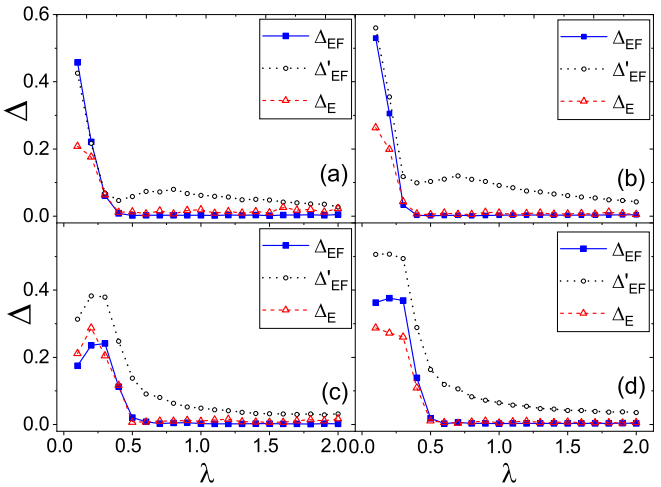

FIG. 5. "Distance" to chaos in the LMG model and the Dicke model. The measures Δ_{EF} (solid squares) in Eq. (30) and Δ'_{EF} (open circles) in Eq. (59) are computed from statistical properties of EFs and the measure Δ_E (open triangles) in Eq. (32) is computed from the statistics of spectra. (a) The LMG model with $\Omega = 80$, (b) the LMG model with $\Omega = 1000$, (c) the Dicke model with $N = 80$, and (d) the Dicke model with $N = 1000$. The effective Planck constants are given by $1/\Omega$ and $1/N$, respectively, in the two modes. The two measures Δ_{EF} and Δ_E give almost the same results for the "distance" to chaos, when the systems are not far from chaos.

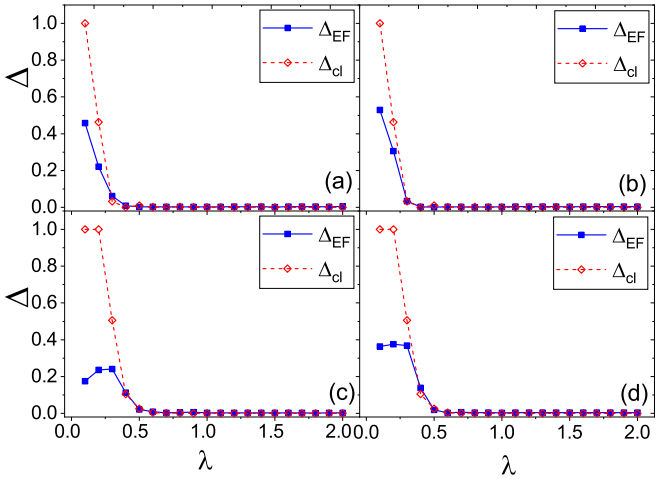

FIG. 6. "Distances" to classical and quantum chaos in the LMG model and the Dicke model. The measure Δ_{EF} (solid squares) is the same as that in Fig. 5. The measure Δ_{cl} (open diamonds) is defined in Eq. (60) and was computed from properties of the corresponding classical phase spaces. (a) The LMG model with $\Omega = 80$, (b) the LMG model with $\Omega = 1000$, (c) the Dicke model with $N = 80$, and (d) the Dicke model with $N = 1000$.

The difference between $\langle|C_{\alpha \boldsymbol{n}}|^2\rangle'$ in Eq. (57) and $\langle|C_{\alpha \boldsymbol{n}}|^2\rangle$ in Eq. (24) is quite clear.

In the computation of $g(R')$, only those rescaled components $R'_{\alpha \boldsymbol{n}}$ in the region with nonzero $S(E_\alpha, \boldsymbol{E_n})$ were used. We found that, unlike the case of $f(R)$ discussed above, the distribution $g(R')$ usually shows obvious deviation from $f_G(R')$ when the classical system is in the chaotic regime (Figs. 3 and 4). Here, in the additional average for the unperturbed system, 100 EFs in the middle energy region were used, with $\epsilon_0 \approx 0.645$ in the LMG model and $\epsilon_0 \approx 0.02$ in the Dicke model.

Variation of the measure Δ_{EF} in Eq. (30) with the controlling parameter λ is given in Fig. 5, together with the often-used measure given by Δ_E of the statistics of spectra. In order

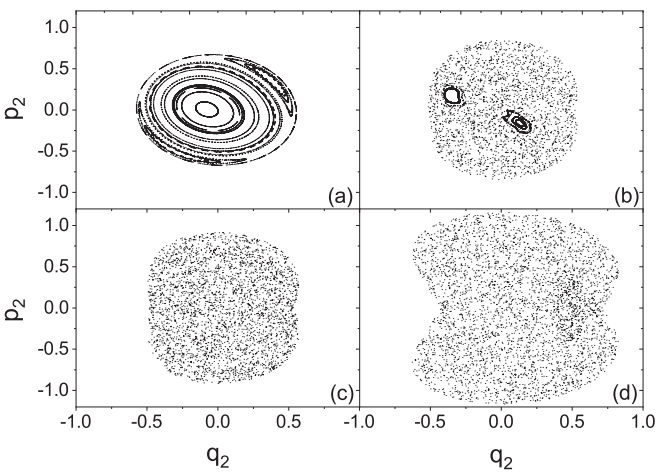

FIG. 7. Poincaré surfaces of section in the LMG model for $E = 12 + \sqrt{2}$ and $q_1 = 0$. (a) $\lambda = 0.1$; (b) $\lambda = 0.3$; (c) $\lambda = 0.4$; (d) $\lambda = 1.0$.

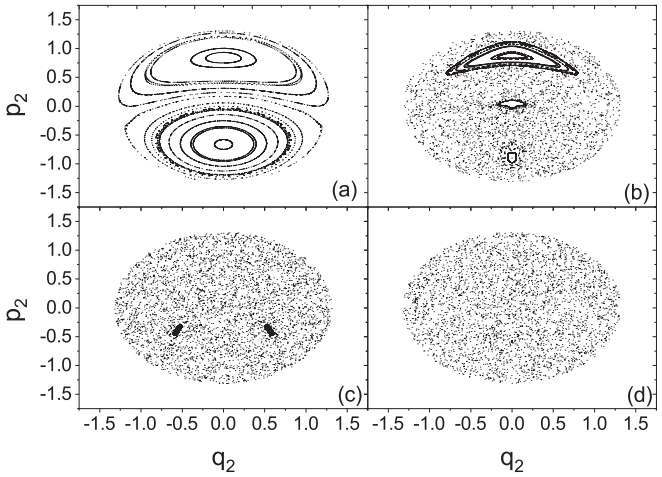

FIG. 8. Poincaré surfaces of section in the Dicke model for $E = \frac{\sqrt{3}-1}{2}$ and $q_1 = 0$. (a) $\lambda = 0.2$; (b) $\lambda = 0.4$; (c) $\lambda = 0.6$; (d) $\lambda = 1.0$.

to improve the statistics, for each value of λ, we used data obtained from several values of λ' in a neighborhood of λ, $\lambda' \in [\lambda - 0.05, \lambda + 0.05]$.

The agreement of the two measures Δ_{EF} and Δ_E is already good in the case of not quite large Ω in the LMG model [Fig. 5(a) with $\Omega = 80$]. The agreement becomes better, when the value of Ω is increased such that the system becomes closer to its classical limit [Fig. 5(b)]. Similar results were also found in the Dicke model [Figs. 5(c) and 5(d)]. Therefore, in these two models, the difference Δ_{EF} can be regarded as a good measure for the "distance" to chaos.

For comparison, we have also computed the difference Δ'_{EF} given by the other rescaling procedure,

$$\Delta'_{EF} = \int |I_g(R') - I_{f_G}(R')|\, dR', \tag{59}$$

where $I_g(R')$ denotes the cumulative distribution for $g(R')$. Due to the obvious difference between the distribution $g(R')$ and the Gaussian distribution shown in Figs. 3 and 4, one expects a notable difference between Δ'_{EF} and Δ_E. Indeed, as shown in Fig. 5, unlike the case with Δ_{EF} discussed above, the agreement between Δ'_{EF} and Δ_E is not good.

We have also computed a "distance" to chaos in the classical counterparts, denoted by Δ_{cl}, which measures the proportion of regular region in energy surface. The measure is defined by

$$\Delta_{cl} = \lim_{N_T \to \infty} \frac{N_R}{N_T}, \tag{60}$$

where N_T is a total number of points taken randomly in an energy surface of interest and N_R is the number of the points for which $\lambda_L < \lambda_m$. Here λ_m is some small quantity and λ_L is the Lyapunov exponent, defined as follows in the long time limit:

$$\lambda_L = \lim_{t \to \infty} \lim_{d_0 \to 0} \frac{1}{t} \ln \frac{|d_t|}{|d_0|}, \tag{61}$$

where d_0 denotes the initial phase-space distance and d_t denotes the distance at a time t. In our numerical simulation, we took $t = 1000$, $N_T = 5000$, $\lambda_m = 0.02$ in the LMG model and $t = 50\,000$, $N_T = 5000$, $\lambda_m = 0.001$ in the Dicke model.

In Fig. 6 it is seen that the agreement between the distances to quantum and classical chaos, characterized by Δ_{EF} and Δ_{cl}, respectively, is quite good. Some examples of Poincaré surfaces of sections in the two models are shown in Figs. 7 and 8.

IV. NUMERICAL SIMULATIONS IN MODELS WITHOUT CLASSICAL COUNTERPARTS

In this section, we study the distribution of rescaled components of EFs in models without any classical counterpart. It seems reasonable to expect that the final result of Sec. II A, that is, that the distribution of appropriately rescaled components should have a Gaussian form, may be valid to some extent in this type of models as well.

Here a major problem met is the determination of the region of components that should be taken into account. As discussed previously, in a system with a classical counterpart, this region corresponds to the classically energetically allowed region. For a system without any classical counterpart, this is a highly nontrivial problem. In this paper, we do not intend to solve this problem but to circumvent it by restricting ourselves to models whose EFs occupy almost the whole unperturbed energy region. In this type of models, one can simply use all components of the EFs when computing $f(R)$. Specifically, we study a defect XXZ model and a defect Ising model, adopting a periodic boundary condition in numerical simulations.

The defect XXZ model [37] is a modified XXZ model, in which an external magnetic field is applied on two sites of the N spins. The unperturbed Hamiltonian and the perturbation have the following forms:

$$H_0 = \sum_{i=1}^{N} s_x^i s_x^{i+1} + s_y^i s_y^{i+1} + \mu_z \sum_{i=1}^{N} s_z^i s_z^{i+1} \tag{62}$$

$$V = \mu_1 s_z^1 + \mu_4 s_z^4, \tag{63}$$

where the periodic boundary condition implies that $s_a^{N+1} = s_a^1$ for $a = x,y,z$. The system is a quantum chaotic system for λ within an appropriate regime, while it exhibits the so-called many-body localization for λ sufficiently large. The Hamiltonian H is commutable with S_z, the z component of the total spin, and we consider a subspace with a definite value of S_z in our numerical study. Other parameters used in this model are $\mu_1 = 1.11$, $\mu_4 = 1.61$, and $\mu_z = 1$.

The defect Ising model is a transverse Ising model, in which an additional magnetic field is applied on two sites of the N spins, with

$$H_0 = \sum_{i}^{N} s_z^i s_z^{i+1} + \mu_x \sum_{i=1}^{N} s_x^i, \tag{64}$$

$$V = \mu_1 s_z^1 + \mu_4 s_z^4. \tag{65}$$

Similarly, it is a quantum chaotic system for λ in an appropriate regime and exhibits many-body localization for λ sufficiently large. The parameters used are $\mu_1 = 1.11$, $\mu_4 = 1.61$, and $\mu_x = 0.6$.

Our numerical simulations reveal that, in these two models, the distributions $f(R)$ are also quite close to the Gaussian form $f_G(R)$, when the statistics of the spectra is close to the prediction of RMT as illustrated in Fig. 9 with $\lambda = 0.5$. Unlike the two models discussed in the previous section, the distributions $g(R')$ are also close to the Gaussian form at $\lambda = 0.5$.

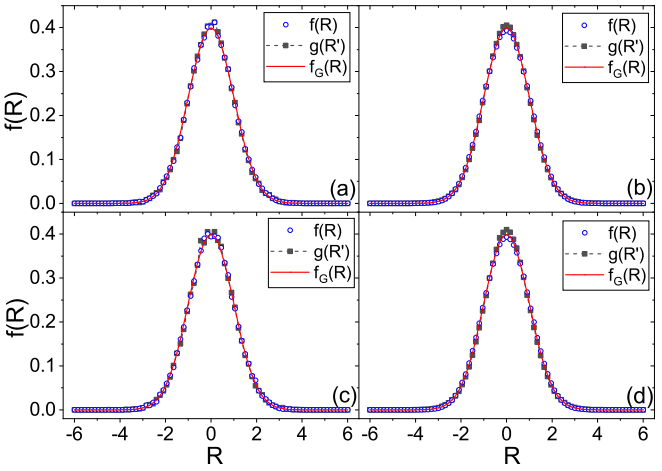

FIG. 9. The distribution $f(R)$ (open circles) and $g(R')$ (solid blocks with dashed lines) for $\lambda = 0.5$ in the defect Ising model and the defect XXZ model. The solid curve indicates the Gaussian distribution $f_G(R)$. (a) The defect Ising model with $N = 10$; (b) the defect Ising model with $N = 15$; (c) the defect XXZ model with $N = 12$ and $S_z = -1$; (d) the defect XXZ model with $N = 19$ and $S_z = -3.5$.

In the computation of $f(R)$, 50 EFs in the middle energy region were used. The energy windows ϵ are as follows: In the defect Ising model, $\epsilon \approx 0.2$ and $\epsilon_0 = 0.02$ for $N = 10$ in contrast to the total energy domain $\Delta E = 7.11$, and $\epsilon \approx 0.07$

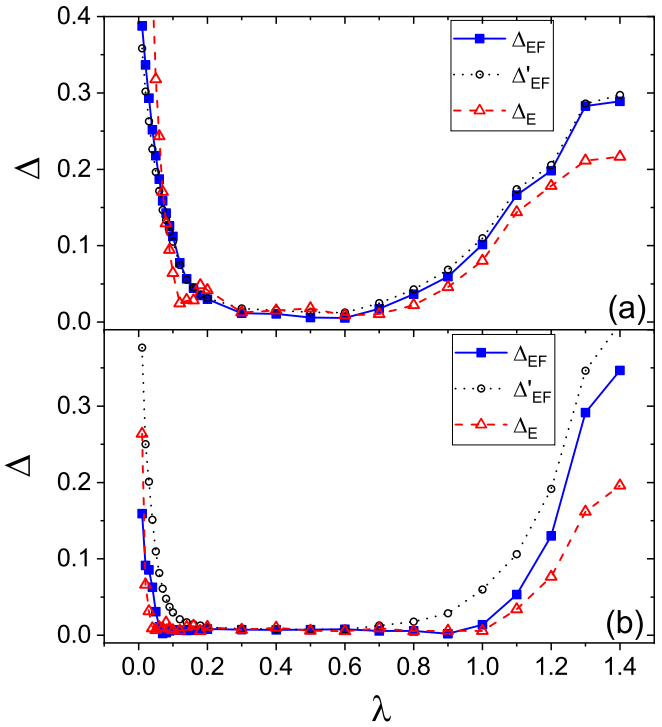

FIG. 10. Similar to Fig. 5, but for the defect Ising model with (a) $N = 10$ and (b) $N = 15$.

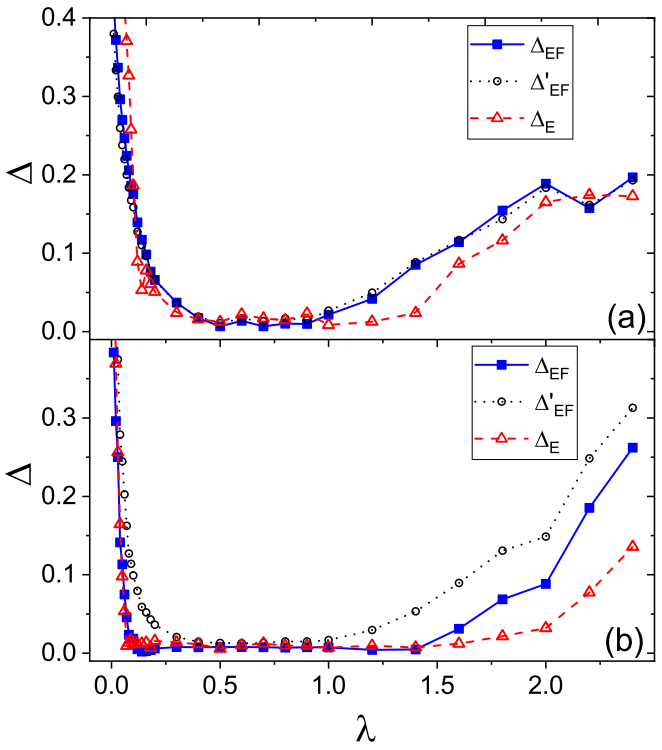

FIG. 11. Similar to Fig. 5, but for the defect XXZ model with (a) $N = 12$, $S_z = -1$, and (b) $N = 19$, $S_z = -3.5$.

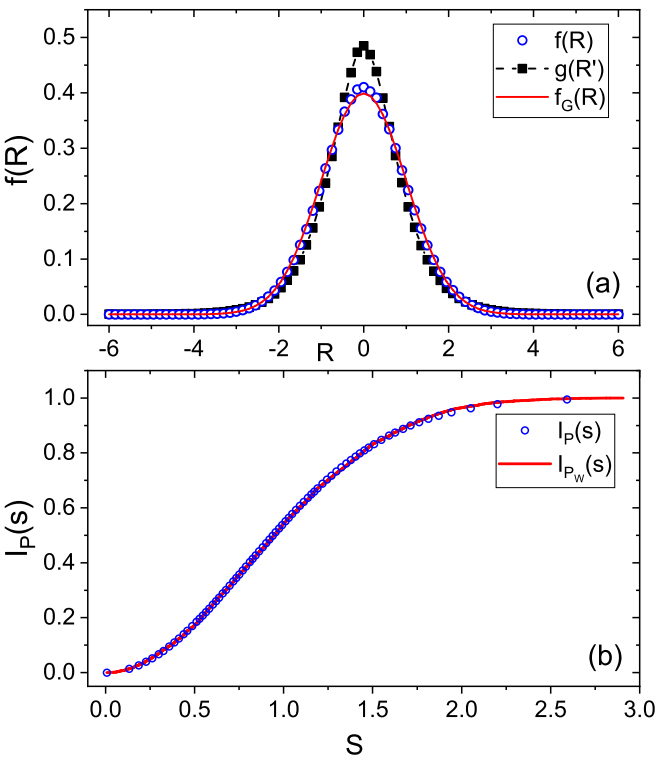

FIG. 12. (a) The distributions of $f(R)$ (open circles) and $g(R')$ (solid blocks with dashed lines) in the defect Ising model with $N = 15$ and $\lambda = 0.06$. (b) The corresponding cumulative distribution of the nearest-level-spacing distribution (open circles). The solid curve indicates the cumulative distribution given by the Wigner surmise.

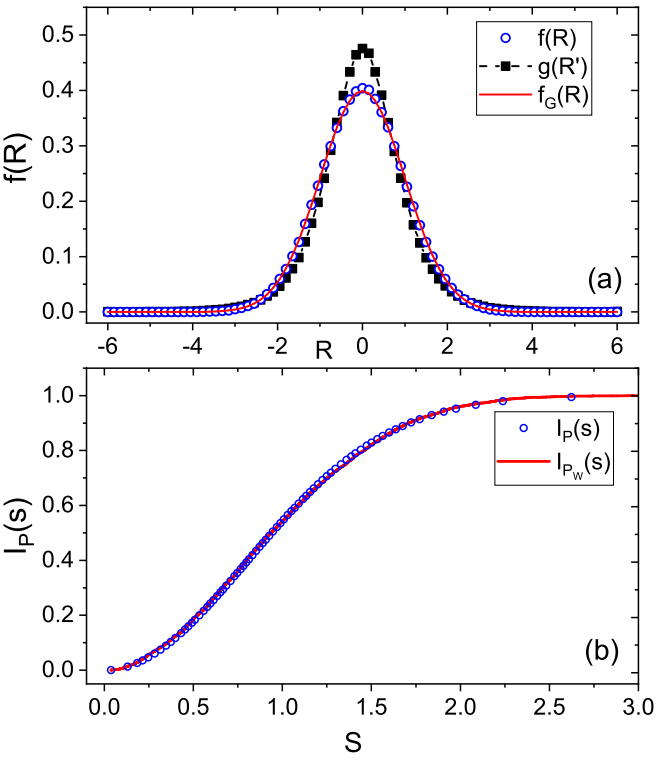

FIG. 13. Similar to Fig. 12, but for the defect XXZ model with $N = 19$, $S_z = -7$, and $\lambda = 0.12$.

for $N = 15$ in contrast to $\Delta E = 10.64$; in the defect XXZ model, $\epsilon \approx 0.3$ and $\epsilon_0 = 0.02$ for $N = 12$, $S_z = -1$ in contrast to $\Delta E = 8.03$, and $\epsilon \approx 0.01$ for $N = 19$, $S_z = -3.5$ in contrast to the total energy domain $\Delta E = 10.66$.

The two measures Δ_{EF} and Δ_E exhibit similar behaviors, like the cases discussed in the previous section for the LMG and Dicke models (Figs. 10 and 11). Thus, at least in these two models, the difference Δ_{EF} can be regarded as a good measure for the "distance" to chaos.

Consistent with the behaviors of the distribution $g(R')$ illustrated in Fig. 9, the two quantities Δ'_{EF} and Δ_{EF} are close in most regions where the systems are chaotic systems according to their spectra statistics. That is, in most cases, an average over the unperturbed energy does not bring much difference in the defect Ising and defect XXZ models. This may be partially related to the fact that EFs in these two models occupy almost the whole energy region for λ not small.

There are still some regions of λ in Figs. 10(b) and 11(b) with relatively large Hilbert spaces, in which Δ'_{EF} shows some notable deviation from Δ_{EF} and Δ_E. Some examples of the distributions $f(R)$ and $g(R')$ in this case are shown in Figs. 12 and 13, together with the corresponding distributions of $I_P(s)$ and $I_{P_W}(s)$.

V. CONCLUSIONS

In this paper, based on semiclassical analysis, it has been shown that those components of EFs of quantum chaotic systems which lie in classically allowed regions of integrable bases can be regarded as random numbers in a sense similar to that stated in the Berry's conjecture. For the distribution

$f(R)$ of these components to have a Gaussian form, which is predicted by the RMT, an appropriated rescaling procedure with respect to the average shape of EFs is needed, where the average should be taken over perturbed states with neighboring energies. It is found that an additional average over unperturbed basis states with neighboring unperturbed energies may cause deviation of the distribution of rescaled components of EFs from the Gaussian form.

The above results suggest that deviation of the distribution $f(R)$ from the Gaussian distribution may be used as a measure for the "distance" to quantum chaos. In two models possessing classical counterparts, when the perturbed system goes from integrable to chaotic with the increase of perturbation strength, our numerical simulations show that this deviation coincides with the deviation of the nearest-level-spacing distribution from the prediction of RMT.

It is known that specific dynamics of the underlying classical systems may induce certain modifications to the Berry's conjecture [38–45]. Since the main result of this paper is based on this conjecture, specific underlying classical dynamics may have some influence in results of this paper as well. In particular, it may induce some deviation of the distribution $f(R)$ for some EFs from the Gaussian distribution. However, if sufficiently many EFs are used in the computation of $f(R)$, it is reasonable to expect that the induced deviation should be small.

In two models without simple classical counterpart, we have found similar numerical results about the distribution of $f(R)$. Analytical explanation of this point is still lacking. It seems that the following feature of these two models may be of relevance. That is, in both models the matrices of the perturbations V in the unperturbed bases do not have a clear band structure; in other words, the perturbation couples basis vectors far separated in energy. We hope that these numerical results may stimulate more investigations.

ACKNOWLEDGMENT

This work was partially supported by the Natural Science Foundation of China under Grant Nos. 11275179, 11535011, and 11775210.

[1] M. V. Berry, J. Phys. A: Math. Gen. **10**, 2083 (1977); Proc. R. Soc. London, Ser. A **400**, 229 (1985).
[2] M. V. Berry, in *Les Houches LII, Chaos and Quantum Physics*, edited by M.-J. Giannoni, A. Voros, and J. Zinn-Justin (North-Holland, Amsterdam, 1991), pp. 251–303.
[3] *Quantum Chaos: Between Order and Disorder*, edited by G. Casati and B. V. Chirikov (Cambridge University Press, Cambridge, 1994).
[4] F. Haake, *Quantum Signatures of Chaos*, 3rd ed. (Springer-Verlag, Berlin, 2010).
[5] D. C. Meredith, S. E. Koonin, and M. R. Zirnbauer, Phys. Rev. A **37**, 3499 (1988).
[6] V. V. Flambaum, G. F. Gribakin, and F. M. Izrailev, Phys. Rev. E **53**, 5729 (1996); J. Phys. A **29**, 5817 (1996).
[7] W.-G. Wang, F. M. Izrailev, and G. Casati, Phys. Rev. E **57**, 323 (1998).
[8] H.-J. Stöckmann, *Quantum Chaos: An Introduction* (Cambridge University Press, Cambridge, 1999).
[9] Y. Alhassid, Rev. Mod. Phys. **72**, 895 (2000).
[10] G. Hackenbroich, C. Viviescas, B. Elattari, and F. Haake, Phys. Rev. Lett. **86**, 5262 (2001).
[11] W.-G. Wang, Phys. Rev. E **65**, 036219 (2002).
[12] M. Horvat and T. Prosen, J. Phys. A **36**, 4015 (2003).
[13] H. Olofsson, S. Aberg, O. Bohigas, and P. Leboeuf, Phys. Rev. Lett. **96**, 042502 (2006).
[14] S. Gnutzmann, J. P. Keating, and F. Piotet, Ann. Phys. **325**, 2595 (2010).
[15] A. M. Smith and L. Kaplan, Phys. Rev. E **80**, 035205 (2009); **82**, 016214 (2010).
[16] J. M. Deutsch, Phys. Rev. A **43**, 2046 (1991).
[17] M. Srednicki, Phys. Rev. E **50**, 888 (1994).
[18] M. Rigol, V. Dunjko, and M. Olshanii, Nature (London) **452**, 854 (2008).
[19] L. F. Santos, F. Borgonovi, and F. M. Izrailev, Phys. Rev. Lett. **108**, 094102 (2012); Phys. Rev. E **85**, 036209 (2012).
[20] A. Altland and F. Haake, Phys. Rev. Lett. **108**, 073601 (2012).
[21] M. Rigol and M. Srednicki, Phys. Rev. Lett. **108**, 110601 (2012).
[22] A. Khodja, R. Steinigeweg, and J. Gemmer, Phys. Rev. E **91**, 012120 (2015).
[23] L. D'Alessio, Y. Kafri, A. Polkovnikov, and M. Rigol, Adv. Phys. **65**, 239 (2016).
[24] F. Borgonovi, F. M. Izrailev, L. F. Santos, and V. G. Zelevinsky, Phys. Rep. **626**, 1 (2016)
[25] V. Buch, R. B. Gerber, and M. A. Ratner, J. Chem. Phys. **76**, 5397 (1982).
[26] L. Benet, J. Flores, H. Hernandez-Saldana, F. M. Izrailev, F. Leyvraz, and T. H. Seligman, J. Phys. A **36**, 1289 (2003).
[27] J. Wang and W.-G. Wang, Chaos Solitons Fractals **91**, 291 (2016).
[28] A. Voros, Ann. Inst. Henri Poincaré A **24**, 31 (1976).
[29] A. Voros, Ann. Inst. Henri Poincaré A **26**, 343 (1977).
[30] F. Borgonovi, I. Guarneri, and F. M. Izrailev, Phys. Rev. E **57**, 5291 (1998).
[31] L. Benet, F. M. Izrailev, T. H. Seligman, and A. Suárez-Moreno, Phys. Lett. A **277**, 87 (2000).
[32] The distribution of rescaled components computed in Ref. [27] is for the so-called nonperturbative regions of EFs. The relation between these regions and classically allowed regions will be discussed in a different paper.
[33] H. J. Lipkin, N. Meshkov, and A. J. Glick, Nucl. Phys. **62**, 188 (1965).
[34] X. Gong-ou, G. Jiang-bin, W. Wen-ge, Y. Ya-tian, and F. De-ji, Phys. Rev. E **51**, 1770 (1995).
[35] R. H. Dicke, Phys. Rev. **93**, 99 (1954).
[36] C. Emary and T. Brandes, Phys. Rev. E **67**, 066203 (2003).
[37] E. J. Torres-Herrera and L. F. Santos, Phys. Rev. E **89**, 062110 (2014).
[38] E. J. Heller, Phys. Rev. Lett. **53**, 1515 (1984).
[39] P. O'Connor, J. Gehlen, and E. J. Heller, Phys. Rev. Lett. **58**, 1296 (1987).

[40] M. Srednicki, Phys. Rev. E **54**, 954 (1996).
[41] S. Hortikar and M. Srednicki, Phys. Rev. E **57**, 7313 (1998).
[42] W. E. Bies, L. Kaplan, M. R. Haggerty, and E. J. Heller, Phys. Rev. E **63**, 066214 (2001).
[43] A. Bäcker and R. Schubert, J. Phys. A **35**, 539 (2002).
[44] J. D. Urbina and K. Richter, J. Phys. A **36**, L495 (2003); Phys. Rev. E **70**, 015201 (2004); Phys. Rev. Lett. **97**, 214101 (2006).
[45] L. Kaplan, Phys. Rev. E **71**, 056212 (2005).